Supporting Information

Tri(ethylene glycol) Divinyl Ether-Crosslinked Gel Polymer Electrolyte Membrane with Enhanced Alkaline Stability and Electrolyte Retention for Flexible Zinc–Air Batteries

Vandana Kumari, Gaganjot, Monica Katiyar *

Department of Materials Science & Engineering,

National Centre for Flexible Electronics, and

Samtel Centre for Display Technology,

Indian Institute of Technology, Kanpur, U.P. – 208016, India

* Correspondence: mk@iitk.ac.in

1. Experimental section

1.1 Materials

Acrylic acid (AA), PEO (M_w~6,00,000), tri (ethylene glycol) divinyl ether (TEGDE), 2-Hydroxy-4′-(2-hydroxyethoxy)-2-methylpropiophenone, also known as IGRA-cure 2959, were obtained from Sigma Aldrich. Potassium hydroxide (KOH) pellets (85% purity AR grade) were procured from Loba Chemies. Carbon cloth (0.4 mm thickness) was purchased from the Fuel cell store. Zinc foil (~0.2 mm thickness, 99.98% metal basis) obtained from ThermoFisher Scientific. Cobalt (III) oxide (Co_3O_4), Nafion solution (25 %) and isopropanol were purchased from Sigma Aldrich.

1.2 Synthesis of gel polymer electrolyte

The composition and synthesis steps of the optimized (PI2.5-AA10-TEGDE10-PEO25) GPE are discussed as follows. Initially, 2 g of acrylic acid (AA), corresponding to 10 wt% of the total solution weight, was dissolved in 16 mL of deionized water. The acrylic acid underwent complete neutralization to adjust the pH of the AA solution to 7 by employing equal moles of KOH (1.557 g) and AA, followed by stirring for one hour to obtain the potassium acrylate solution. Subsequently, 25 wt% of PEO (0.5 g) polymer filler relative to the weight of the AA monomer was added into the potassium acrylate solution, and the mixture was stirred for approximately 2 hours, resulting in a homogeneously viscous solution. The clear solution was degassed under nitrogen to eliminate the dissolved oxygen. 10 wt% TEGDE (200 μL) crosslinker relative to AA monomer was included and allowed to mix vigorously overnight for homogeneous dissolution. Finally, 2.5 wt% (50 mg) IRGA-cure 2959 relative to AA monomer was included in the solution and stirred for one hour. The resultant solution was then degassed to remove any dissolved oxygen prior to final casting onto a polypropylene (PP) tray for photo-polymerization. Subsequently, the resulting solution was placed in a PP tray and subjected to photo-initiated free radical polymerization through exposure to UV light (3 $mWcm^{-2}$) for a duration of 2 hours. All steps were carried out at room temperature. The membrane was dried at room temperature and subsequently immersed in a 6M KOH solution for 24 hours until the electrolyte uptake attained saturation, thus preparing the hydrogel electrolyte membrane. In a similar manner, the Potassium Polyacrylate (PAAK) GPE membrane was synthesized for comparison purposes.

1.3 Physical characterization and measurement

1.3.1 Characterization

The Fourier transform infrared (FTIR) spectra were recorded using a PerkinElmer instrument, covering the wavenumber range of 400 to 4000 cm^{-1} at room temperature. Raman measurements were conducted utilizing the Princeton Instrument Spectra Pro2500i, which is equipped with a laser diode operating at 533 nm, covering the wavelength range of 700 to 3100 cm^{-1} at room temperature. The XRD measurements were conducted with a Panalytical X'Pert Empyrean X-ray diffractometer, functioning at 40 kV and 45 mA, utilizing Ni-filtered Cu Kα radiation (1.5406 Å) at a scan rate of 2°

min^{-1} to investigate the crystal structure of the membrane and its associated components. Tungsten scanning electron microscopy (SEM, JEOL, 10 kV) was utilized to observe the morphologies of the gel electrolyte membrane. To study the surface morphology of as prepared membrane, it was dried at 40 °C to eliminate moisture from the membrane. As prepared membrane was saturated with water and freeze-dried to analyze the 3D network structure formation of the membrane using SEM.

1.3.2 Mechanical testing

The mechanical properties of GPEs samples (3×1 cm) were tested using universal testing machine (Zwick Roell Z005 Testing Machine Technology Co. Ltd.) with a tensile speed of 20 mm min^{-1} and maximum test load of 5kN at room temperature.

1.3.3 Liquid uptake and retention capacity tests

The liquid uptake (6M KOH electrolyte solution) and retention capacities were investigated in air at 25 °C and 45% of relative humidity. The dried membrane (mass m_0) was soaked in electrolyte solution for a different measurement time. Then, the excess solution on the sample surface was wiped off with filter paper, and the sample was weighed again (mass m_1). The liquid uptake rate was calculated by formula ($W_{up}\%=(m_1-m_0)/m_0 * 100\%$).

To evaluate the liquid retention (6M KOH solution) capacity, liquid-saturated GPE (mass w_2) was subsequently exposed to air at 25 °C. The weight (mass w_3) of each sample was monitored over time. The liquid retention rate was calculated by the formula ($R\%= m_3/m_2 * 100\ \%$).

1.4 Electrochemical performance of GPEs and ZABs

1.4.1 Preparation of air electrode

To increase the wettability of hydrophobic carbon cloth gas diffusion layer (GDL), an oxygen plasma treatment was applied to catalyst deposition side of carbon cloth so that it can absorb water-based catalyst ink efficiently. Following the surface treatment of carbon cloth with geometric area of 2 cm^2, the air electrode is prepared by drop casting the catalyst ink to load the catalyst onto the carbon cloth. The catalyst ink consists of 50 mg Co_3O_4 catalyst powder, 40 mg activated carbon, 40 μL Nafion solution (25 wt. %, Aldrich) in 6 mL DI water, and 3 mL isopropanol. The catalyst ink was dropped cast through micropipette onto the carbon cloth immediately after its O_2 plasma treatment for 1 minute and then dried at 40 °C for 2 hours, achieving a mass loading of 1 mg cm^{-2}.

1.4.2 Electrochemical measurements

Electrochemical measurements were carried out with a potentiostat (Ametek PGSTAT302N), an electrochemical workstation and Neware Battery Testing system. The ionic conductivities of the 6M KOH saturated GPEs were measured by electrochemical impedance spectroscopy (EIS) with an applied 5 mV AC potential from 100 kHz to 0.1 Hz using two-electrode system. The gels were sandwiched within two stainless steel (SS) coin cell spacers (500 micron) acts as blocking electrodes.

The ionic conductivity was evaluated by the formula $\sigma = {}^{t}/(R_b \times A)$, where t, A and Rb refer to thickness (cm) of GPE, contact area (cm2) of the GPE and the bulk resistance (ohm), respectively. The intrinsic resistance of the GPE was determined from the intercept of the Nyquist plot on the real axis (x-axis) at high frequencies. Four samples were tested for each composition, and the corresponding error values were calculated.

The pouch-type ZAB consisted of carbon cloth coated with Co_3O_4 serving as the air cathode, a GPE membrane saturated with 6M KOH, zinc foil, and packaging materials (see fig. 5a). The zinc foil was polished prior to the assembly of the ZAB. The catalyst-loaded carbon cloth, i.e. air electrode was taken 1x2 cm^2, electrolyte was 1.5 x 2.5 cm^2 and zinc foil 1 x 2 cm^2 was cut in given size. The assembly process is to assemble them layer by layer and subsequently encapsulate the battery using the top side sealing machine.

Galvanostatic discharge and charge measurements were carried out at 1 mA cm^{-2} for 15 min per cycle under ambient conditions to evaluate the performance of the pouch-type ZAB cells. The rate performance was determined at the current densities of 0.5, 1, 2, 3, 5, 8 and 10 mA cm^{-2}. The cell underwent 10 initial charge–discharge cycles to stabilize the voltage profile before performing GCD measurements at different bending angles for the flexibility test. The energy efficiency of the cell was calculated from the ratio of average discharge to charge voltages obtained from the galvanostatic charge–discharge profiles and is reported at representative cycling stages (initial, intermediate, and late cycles) during long-term cycling.

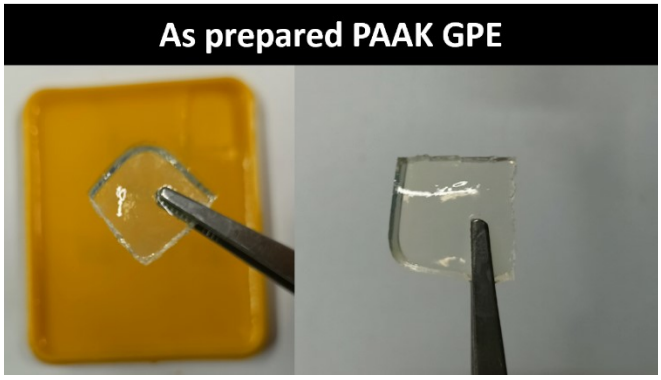

Fig. S1. Digital photograph of as prepared PAAK GPE membrane.

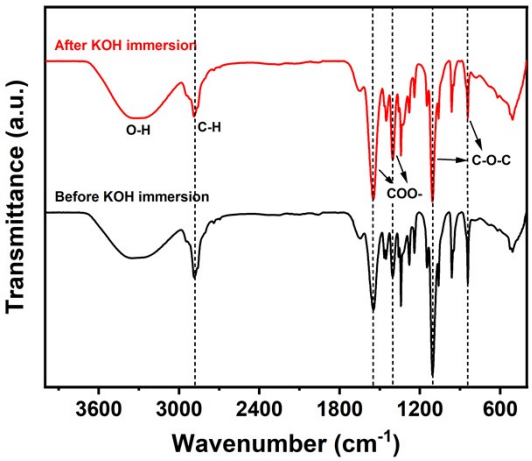

Fig. S2. FT-IR spectra of optimized GPE membrane before and after immersion in 6M KOH solution.

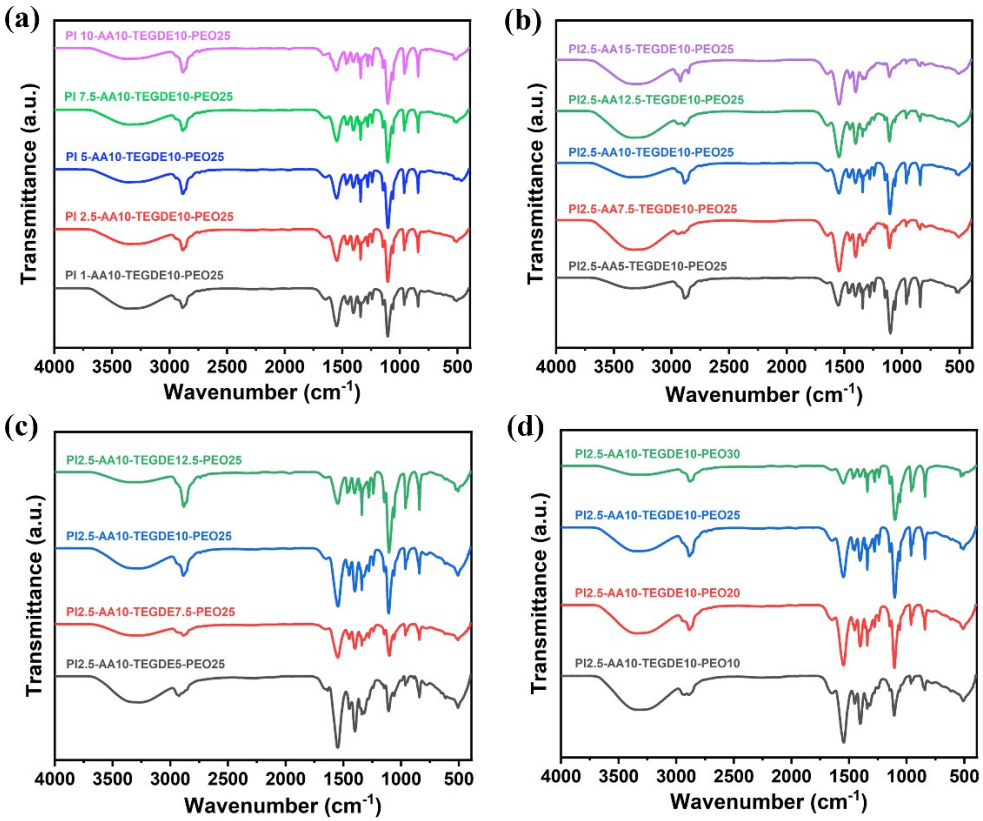

Fig. S3. FT-IR spectra of all GPE membrane compositions.

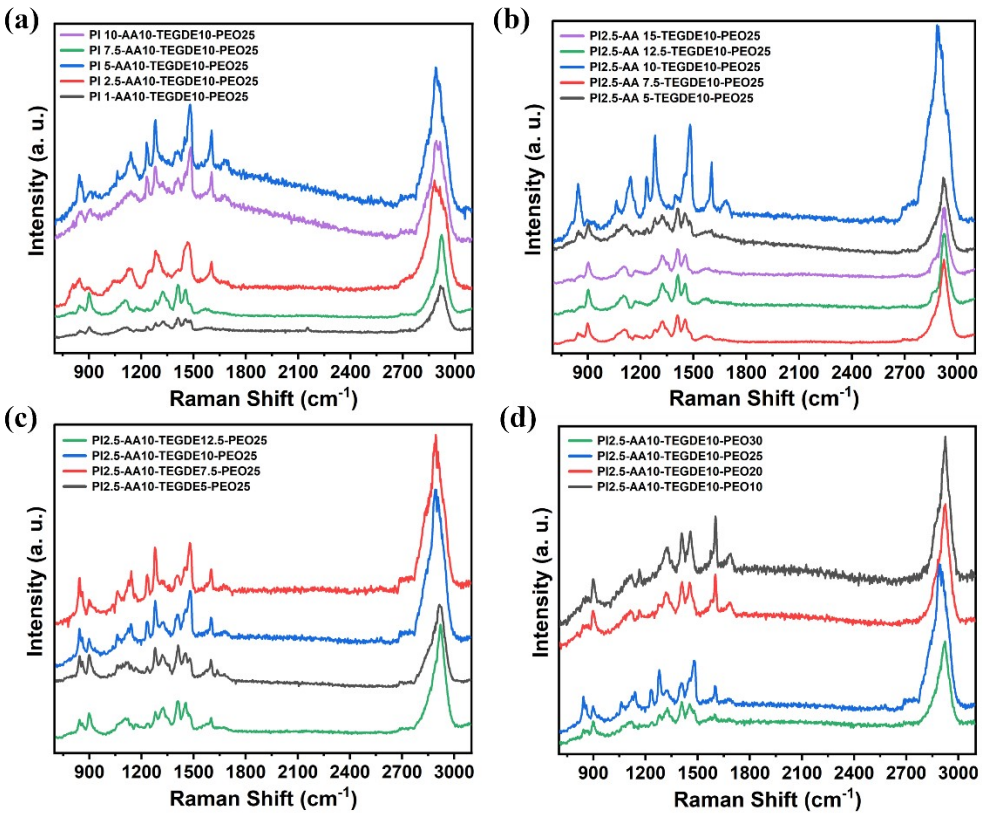

Fig. S4. Raman spectra of all GPE membrane compositions.

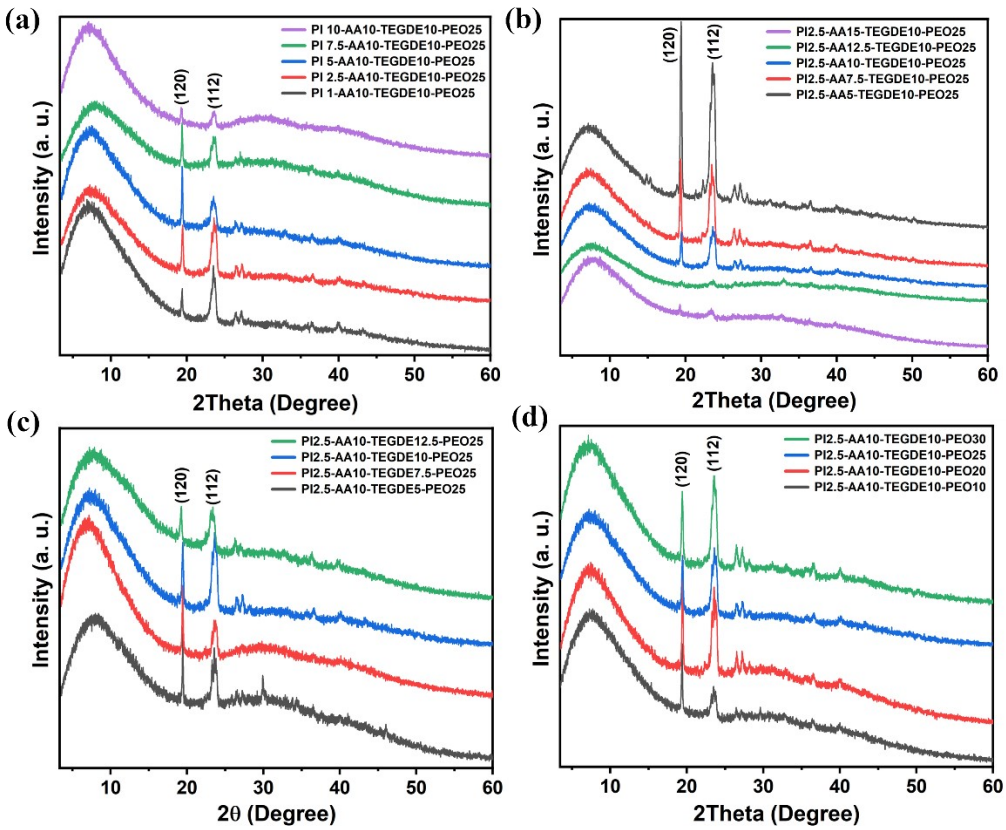

Fig. S5. XRD patterns of all GPE membrane compositions.

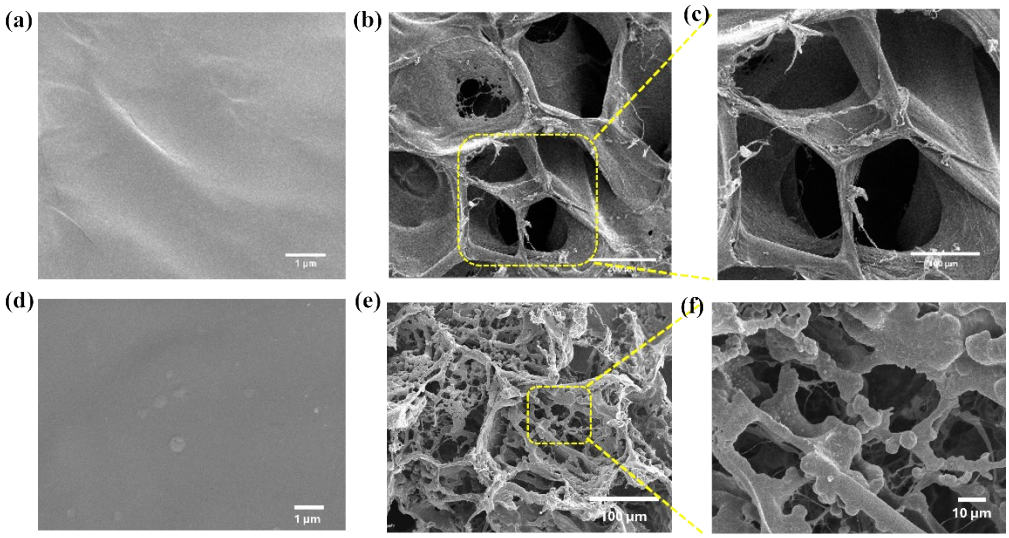

Fig. S6. SEM micrographs of PI2.5-AA10-TEGDE10-PEO25 and PAAK GPE membranes. a and d) dried at ambient condition, b,c,e and f) freeze dried at -80 °C.

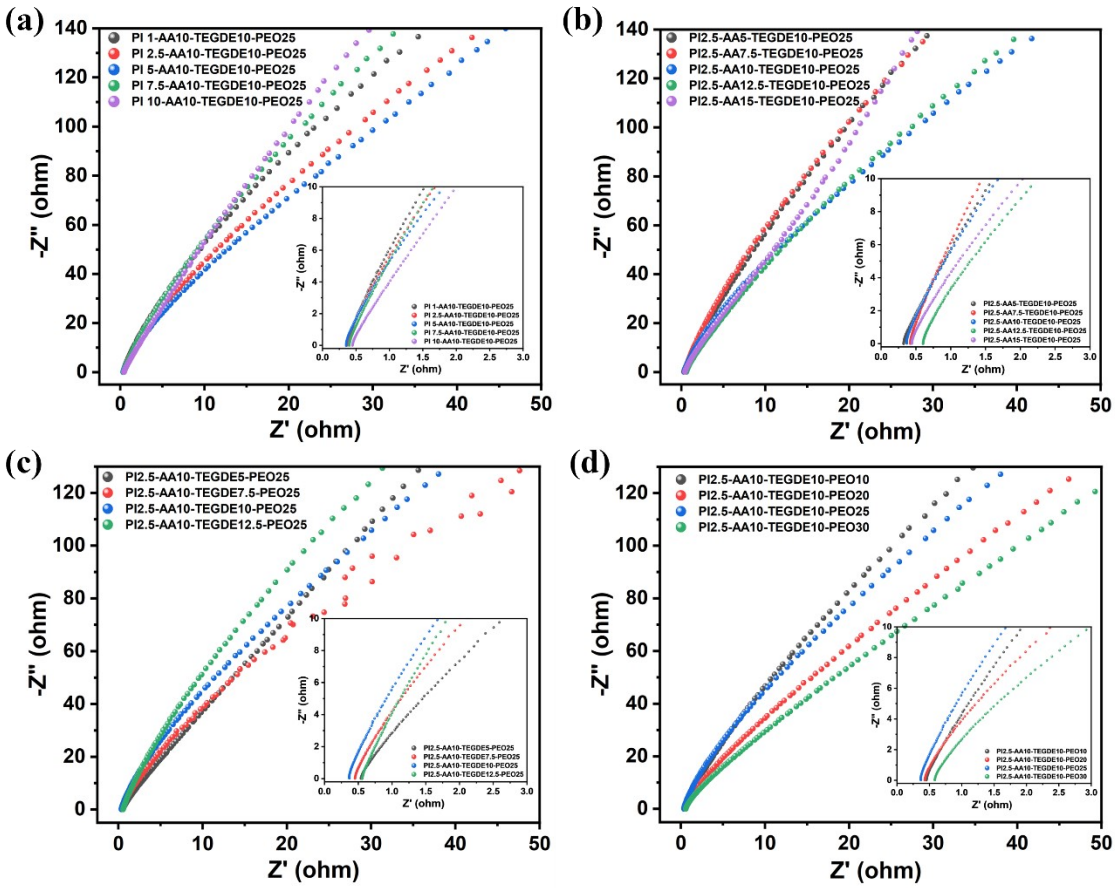

Fig. S7. Nyquist plot of all GPE membranes with different ratio of: a) photo-initiator, b) acrylic acid monomer, c) TEGDE crosslinking agent, and d) PEO polymer filler, respectively.

Table S1. Influence of monomer, photo-initiator, crosslinking agent and polymer filler content on membrane properties of GPE.

Composition code	Film Thickness (mm)	Bulk Resistance R_b (Ω)	Ionic Conductivity ($mScm^{-1}$)	Electrolyte Uptake (%)	Electrolyte Retention % (after 96 hours study)
PI 1-AA10-TEGDE10-PEO 25	2.1	0.376	316 ± 3	370 ± 6	76%
PI 2.5-AA10-TEGDE10-PEO 25	2.2	0.369	339 ± 4	390 ± 3	78%
PI 5-AA10-TEGDE10-PEO 25	2.0	0.354	320 ± 6	379 ± 6	75%
PI 7.5-AA10-TEGDE10-PEO 25	2.0	0.401	282 ± 5	345 ± 2	76%
PI 10-AA10-TEGDE10-PEO 25	2.0	0.450	252 ± 3	336 ± 4	75%
PI 2.5-AA 5-TEGDE10-PEO 25	1.5	0.324	262 ±1	334 ± 17	74%
PI 2.5-AA 7.5-TEGDE10-PEO 25	2.2	0.420	296 ± 2	375 ± 8	76%
PI 2.5-AA 10-TEGDE10-PEO 25	2.2	0.369	339 ± 4	390 ± 3	78%
PI 2.5-AA12.5-TEGDE10-PEO 25	2.8	0.538	289 ± 4	436 ± 6	77%
PI 2.5-AA15-TEGDE10-PEO 25	2.2	0.440	283 ± 2	459 ± 2	77%
PI 2.5-AA10-TEGDE 5-PEO 25	2.2	0.553	225 ± 4	324 ± 6	74%
PI 2.5-AA10-TEGDE 7.5-PEO 25	2.2	0.451	276 ± 6	346 ± 7	76%
PI 2.5-AA10-TEGDE 10-PEO 25	2.2	0.369	339 ± 4	390 ± 3	78%

PI 2.5-AA10-TEGDE 12.5-PEO 25	3.2	0.558	325 ± 4	363 ± 3	77%
PI 2.5-AA10-TEGDE10-PEO 10	2.4	0.456	298 ± 3	462 ± 2	76%
PI 2.5-AA10-TEGDE10-PEO 20	2.4	0.434	313 ± 4	408 ± 1	78%
PI 2.5-AA10-TEGDE10-PEO 25	2.2	0.369	339 ± 4	390 ± 3	78%
PI 2.5-AA10-TEGDE10-PEO 30	2.6	0.585	252 ± 3	355 ± 3	77%

Table S2. Solution resistance (Rs) and charge-transfer resistance (Rct) values extracted from fitted EIS data of the flexible zinc–air cell at different cycling stages.

Cycle number	Rs (Ω)	Rct (Ω)
0	2.37	33.03
60	2.17	11.85
100	2.00	3.32
120	2.63	1.56
150	3.26	0.47
200	3.67	0.45
240	7.71	40.78

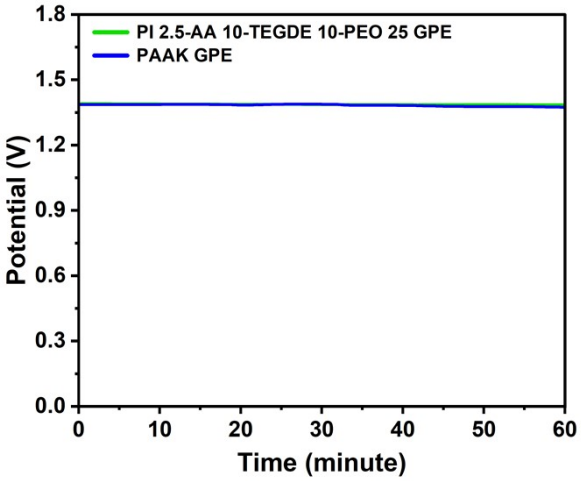

Fig. S8. Open circuit voltage of FZABs.

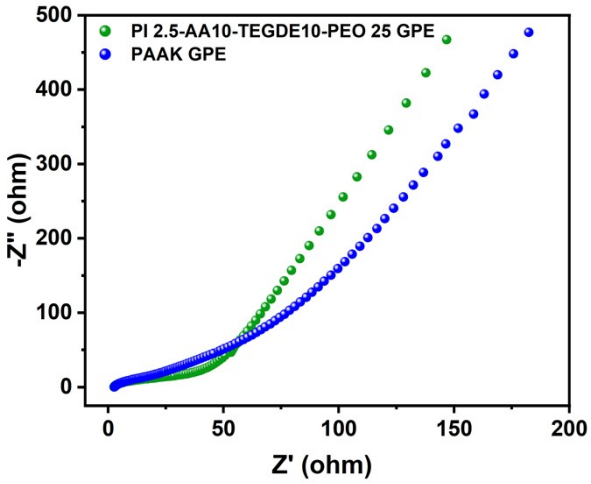

Fig. S9. Nyquist plot of FZABs.

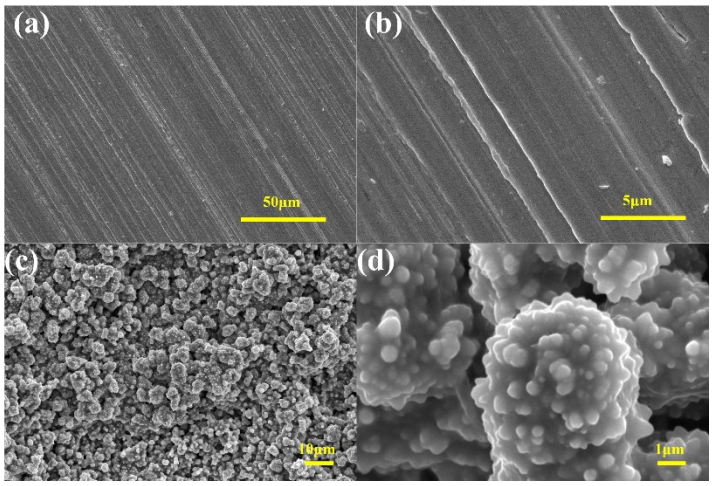

Fig. S10. SEM images of the zinc anode surface: (a, b) polished zinc before cycling at different magnifications; (c, d) zinc surface after prolonged GCD cycling at different magnifications.

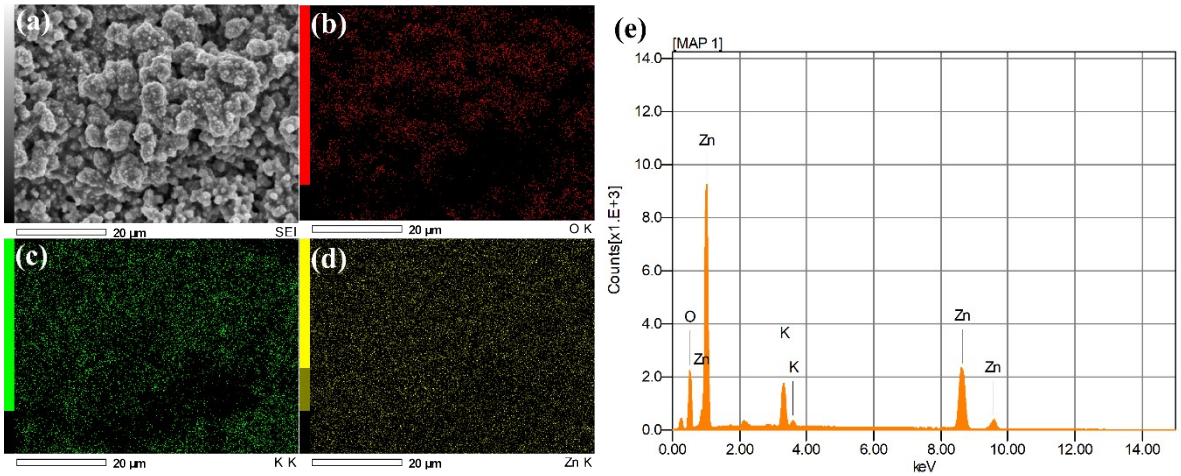

Fig. S11. SEM image and corresponding EDS elemental mapping of the zinc anode after cycling: (a) SEM image; (b) Zn mapping; (c) O mapping; (d) K mapping; (e) EDS spectrum.

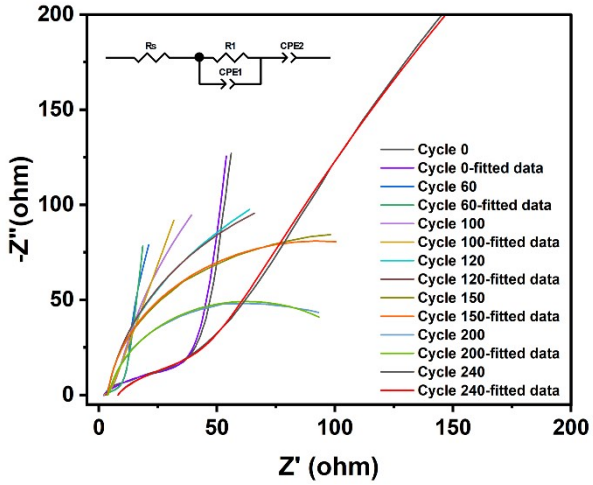

Fig. S12. Nyquist plots of the zinc–air cell at different cycling stages with corresponding fitted curves. Inset shows the equivalent circuit used for fitting.

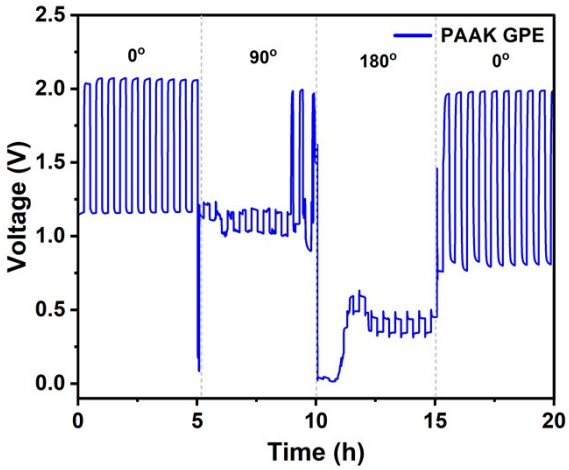

Fig. S13. Galvanostatic discharge and charge at 1 mA cm^{-2} of PAAK GPE-based FZAB at different bending angles.

Table S3. Comparison of GPE-based ZAB performances in this work and some previously reported sandwich-type ZABs.

Catalyst	Electrolyte	Ionic conductivity (mS cm^{-1})	Current density (mA cm^{-2})	Cycling number	Cycling time (h)	Discharge capacity (h)	Ref.
Co_3O_4	**2.5%PI-10%AA-10% TEGDE-25% PEO**	**339**	**1**	**400**	**200 for 30 min/cycle**	**43 at 1 mA cm^{-2}**	**This work**
Pt/C+Ir/C	RPAM-KA	750	1	210	70 for 20 min/cycle	20 at 1 mA cm^{-2}	[1]
Pt/C+IrO_2	PVA-PAAK-PEO	640	2	230	38 for 10 min/cycle	-	[2]
Co_3O_4 @Ni	PANa/CNF/GO NR	268	2	969	323 for 20 min/cycle	-	[3]
Pt/C + RuO_2	PAS-CMC	315	2	180	120 for 40 min/cycle	-	[4]
Pt/C + IrO_2	PVA-PAA-KOH	212	1	189	63 for 20 min/cycle	16.5 at 2 mA cm^{-2}	[5]
MnO_2/Co_3O_4	PVA/N-PAM/KOH	309	2	113	19 for 10 min/cycle	11 at 2 mA cm^{-2}	[6]
Pt/C+Co_3O_4	KI (PVA-PANa-ACG-KI)	283	0.5	186	62 For 20 min/cycle	34	[7]
CoFeP@C	PVAA-Cellulose	123	3	324	54 For 10 min/cycle	-	[8]
Co_3O_4	*n*-PVA–OH–MX	77.6	2	320	160 For 30 min/cycle	-	[9]

MnO_2+ Co_3O_4	RDC/N-PAA/KOH	430	2	75	12.5 For 10 min/cycle	3	[10]
Pt/C + RuO_2	MXene/Zn-LDH-array/PVA	55.3	3	-	50 for 30 min/cycle	-	[11]
Pt/C + Co_3O_4	PVAA–GO–KOH-KI	155	2	200	200 for 60 min/cycle	-	[12]
Pt/Ru/C	PAA-KOH	204	0.5	25	approximately 4.1 for 10 min/cycle	-	[13]
S-doped $CaMnO_3$	PVA–PEO–KOH	-	1	20	10 for 30 min/cycle	-	[14]
Co_3O_4@Ni Fe LDH	PVA–KOH–$Zn(CH_3COO)_2$	-	1.3	120	20 for 10 min/cycle	-	[15]
Co_3O_4/MW CNT	PVA–PAA–KOH	-	0.5	150	25 For 10 min/cycle	-	[16]
NiCo hydroxide	PANa–KOH–$Zn(CH3COO_2$	170	2	800	160 For 12 min/cycle	-	[17]
Co_3O_4	PVA–KOH	-	2	30	10 for 20 min/cycle	2.74	[18]

References:

1 G. Wang, Y. Chi, Y. Zhong, H. Zhou, M. Lu, H. Chen, J. Zhang, E. Hu and Z. Chen, *Chemical Engineering Journal*, DOI:10.1016/j.cej.2025.167644.

2 A. Arredondo-Espínola, L. Álvarez-Contreras, J. Bañuelos-Díaz, M. Guerra-Balcázar, B. L. España-Sánchez and N. Arjona, *J Power Sources*, DOI:10.1016/j.jpowsour.2025.237416.

3 W. Liu, X. Zhao, X. Ye, X. Zheng, Y. Zhang, M. Wang, X. Lin, B. Liu, L. Han, Y. Ning, K. Rui, H. Li and Y. Lu, *Energy and Fuels*, 2024, 38, 6508–6517.

4 Y. Hou, C. Wang, X. Wen, Q. Zhao, H. Liu, J. Zhu, P. Li, X. Yang and K. Zhang, *Chemical Engineering Journal*, DOI:10.1016/j.cej.2024.153817.

5 S. W. Song, H. Kim, S. Shin, S. Jang, J. H. Bae, C. Pang, J. Choi and K. R. Yoon, *Energy Storage Mater*, DOI:10.1016/j.ensm.2023.102802.

6 G. Zhang, X. Cai, C. Li, J. Yao, W. Liu, C. Qiao, G. Li, Q. Wang and J. Han, *ACS Appl Polym Mater*, 2023, 5, 3622–3631.

7 X. Jia, J. Ma, C. Zhang, Z. Zhang, L. Fu and G. Wang, *Electrochim Acta*, DOI:10.1016/j.electacta.2023.142195.

8 W. Li, Y. Wang, R. Liu, W. Chen, H. Zhang and Z. Zhang, *ACS Sustain Chem Eng*, 2023, 11, 3732–3739.

9 Z. Chen, W. Li, X. Yang, C. Ke, H. Chen, Q. Li, J. Guo, Y. He, Z. Guo and X. Liang, *J Power Sources*, DOI:10.1016/j.jpowsour.2022.231020.

10 G. Zhang, X. Cai, C. Li, J. Yao, Z. Tian, F. Zhang, Y. Liu, W. Liu and X. Zhang, *Int J Biol Macromol*, 2022, 221, 446–455.

11 X. Hui, P. Zhang, J. Li, D. Zhao, Z. Li, Z. Zhang, C. Wang, R. Wang and L. Yin, *Adv Energy Mater*, DOI:10.1002/aenm.202201393.

12 Z. Song, J. Ding, B. Liu, X. Liu, X. Han, Y. Deng, W. Hu and C. Zhong, *Advanced Materials*, DOI:10.1002/adma.201908127.

13 T. N. T. Tran, H. J. Chung and D. G. Ivey, *Electrochim Acta*, DOI:10.1016/j.electacta.2019.135021.

14 S. Peng, X. Han, L. Li, S. Chou, D. Ji, H. Huang, Y. Du, J. Liu and S. Ramakrishna, *Adv Energy Mater*, DOI:10.1002/aenm.201800612.

15 X. Guo, X. Hu, D. Wu, C. Jing, W. Liu, Z. Ren, Q. Zhao, X. Jiang, C. Xu, Y. Zhang and N. Hu, *ACS Appl Mater Interfaces*, 2019, 11, 21506–21514.

16 D. Lee, H. W. Kim, J. M. Kim, K. H. Kim and S. Y. Lee, *ACS Appl Mater Interfaces*, 2018, 10, 22210–22217.

17 Y. Huang, Z. Li, Z. Pei, Z. Liu, H. Li, M. Zhu, J. Fan, Q. Dai, M. Zhang, L. Dai and C. Zhi, *Adv Energy Mater*, DOI:10.1002/aenm.201802288.

18 X. Chen, B. Liu, C. Zhong, Z. Liu, J. Liu, L. Ma, Y. Deng, X. Han, T. Wu, W. Hu and J. Lu, *Adv Energy Mater*, DOI:10.1002/aenm.201700779.